



# Effect of Discharge Energy of Magnetic Pulse Compaction on the Powder Compaction Characteristics and Spring Back Behavior of Copper Compacts

Junjia Cui<sup>1</sup> · Xushi Huang<sup>1</sup> · Dongying Dong<sup>1</sup> · Guangyao Li<sup>1</sup>

Received: 13 January 2020 / Accepted: 13 March 2020 / Published online: 11 April 2020  
© The Korean Institute of Metals and Materials 2020

## Abstract

Magnetic pulse compaction (MPC) technology had unique compaction advantages compared to traditional powder compaction methods. In this study, the pure copper compacts have been consolidated by MPC technique. The effect of discharge energy on the microstructures, relative density, micro hardness, strain and stress of copper compacts were analyzed via optical microscopy, scanning electron microscopy, hardness tester and FEM simulation. The relationship between discharge energy and spring back was analyzed by numerical calculation. Results showed that the MPC method had the advantages to refine powder particles. The relative density of copper compacts reached 96% when the discharge energy was 9 kJ. Stress concentration was occurred at the upper edge of the powder body, and propagated to the upper center, lower edge and middle position of the powder body. The powder body could have a uniform strain distribution in a short period of time when the discharge energy was greater than 7 kJ. There was a linear relationship between the relative density and the logarithm of Vickers hardness. The axial and radial spring back both increased with the increase of discharge energy. When the discharge energy was 9 kJ, the axial and radial spring back was 2.36% and 0.42%.

**Keywords** Magnetic pulse compaction · Copper powder · Microstructures · Relative density · Volume strain · Spring back

## 1 Introduction

The powder metallurgy (PM) technology for producing structural parts exhibits many advantages such as high quality, high precision and near-net shape production [1, 2]. In order to obtain PM parts with excellent properties, it is important to develop an efficient powder compaction technology to produce compacts with high density and high performance [3]. In recent years, electromagnetic force has been used for metal forming [4, 5]. The magnetic pulse compaction (MPC) technique was therefore proposed and used to press metal powder and ceramic powder [6, 7]. MPC is a dynamic compaction method and each particle is subjected to a high pressure (up to 5 GPa) during a short period of time

[8]. Compared with the conventional powder compaction methods, the MPC technique has the advantages of short pressing time, slight work hardening and high density of compacts [9]. In view of the advantages and good application prospects, researches have been conducted to study the process parameters of MPC and the properties of compacts.

Copper has been widely used in machine manufacturing, electrical and national defense industries. Therefore, the MPC method has been used to manufacture copper compacts and the performance of copper compacts has been researched. Meng et al. [3] investigated the effects of discharging voltage on density of copper compacts by MPC method. Results showed that the density increased with the increase of discharging voltage. Lee et al. [10] analyzed the effects of compaction temperature on density and hardness by MPC process. Results showed that the density and hardness both increased and then decreased with the increase of compaction temperature. Rhee et al. [11] studied and compared the wear resistance of copper compacts under static and MPC methods. Results showed that the copper compacts fabricated by MPC showed the best wear resistance.

✉ Junjia Cui  
cuijunjia@hnu.edu.cn  
Guangyao Li  
gyli@hnu.edu.cn

<sup>1</sup> State Key Laboratory of Advanced Design and Manufacturing for Vehicle Body, Hunan University, Changsha 410082, China

When the compacts were removed from the die, the elastic inner stress would change the contact state of particles and then cause the volume expansion [12]. Yin et al. [13] analyzed the relationship between radial spring back and impact force by high velocity compaction. Results showed that the radial spring back decreased with the increase of impact force. Amir et al. [14] studied the effects of high power ultrasonic vibrations and grain size on spring back of titanium compacts. Results showed that ultrasonic vibrations could reduce residual internal stresses and the reduction of spring back was about 8.8% in fine powder. An et al. [15] researched the spring back value at different heights of copper compact by FEM simulation. Results showed that the axial spring back increased with the height and the radial spring back at the middle height of the compact was highest.

Continuum models have been used to simulate the powder compaction process [16]. Krok et al. [17] divided the powder bodies with the diameter 8 mm and the height 6 mm into 7700 elements to analyze the thermomechanical behavior. Results showed that the temperature distribution was dramatically changed by the shape of the punch. Khoei et al. [18] used 3D continuum models to study the powder compaction process. Results showed that the inelastic analysis could be effectively used to simulate the powder forming process. Deng et al. [19] researched the residual stress field and densification of Nano diamond powder compacts by finite element analysis. Results showed that the compressive residual stress tended to increase with depth due to multiple shocks.

The above-mentioned studies were mainly focused on the properties of copper compacts at various process parameters (discharge voltage, compaction temperature) of MPC, spring back of compacts at conventional compaction methods and simulation method of powder compaction process. In view of the advantages and good application prospects of MPC, further research was necessary. Discharge energy was an important process parameter of MPC and spring back could impair the strength of compacts. In order to obtain copper compacts with superior properties, it was necessary to understand the compaction characteristics and spring back behavior at various discharge energies. However, the effect of discharge energy on the powder compaction characteristics and spring back behavior of copper compacts was rarely reported.

In this work, the effect of discharge energy on the powder compaction behavior and spring back behavior of copper compacts were investigated. Firstly, microstructures of the copper compacts at various discharge energies were analyzed by environmental scanning electron microscope and metallurgical microscope. Then, the variation tendency of the relative density, strain and stress at various discharge energies were studied by experiment and FEM simulation. Subsequently, micro hardness of copper compacts at various discharge energies was observed. Finally, the effect of

discharge energy on the axial and radial spring back of copper compacts was investigated.

## 2 Magnetic Pulse Compaction Tests

Copper powder with the purity 99.9% was supplied from Shanghai Maoguo Nano technology Co., Ltd., Shanghai, China. The average particle size of the copper powder was 75  $\mu\text{m}$  with typical dendrite morphology, as shown in Fig. 1. MPC experiments were performed on copper powder using a die with 10 mm internal diameter and 40 mm external diameter. The filling height of the powder body was 6 mm and the initial relative density obtained by electronic balance (precision: 0.1 mg) and caliper (precision: 0.02 mm) was about 0.35.

MPC was a kind of dynamic compaction method [8] and the principle of MPC was shown in Fig. 2. The panel coil was fixed and attached to the driving plate, which were both fabricated by pure copper with high conductivity. Specifically, the capacitors in the electromagnetic pulse discharge device were charged to a specified energy before experiment. When the experiment was ready to start, the specified energy was discharged to the panel coil. Then, the panel coil was generated a high-intensity magnetic field and induced an eddy current magnetic field in the driving plate [20, 21]. Finally, the strong repulsive force between the two magnetic fields pushed the driving plate to accelerate downward, causing the upper punch to press the powder particles at a high speed. The powder particles were consolidated in a few milliseconds [8].

MPC experiments were conducted by an electromagnetic pulse device PS48/16 produced by PST Company,

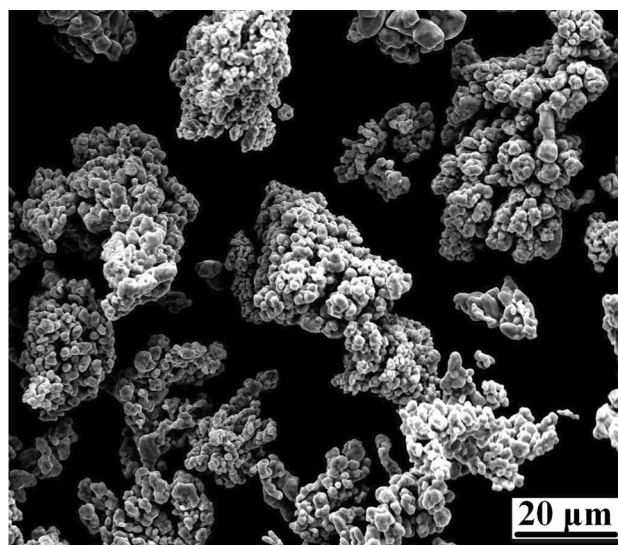
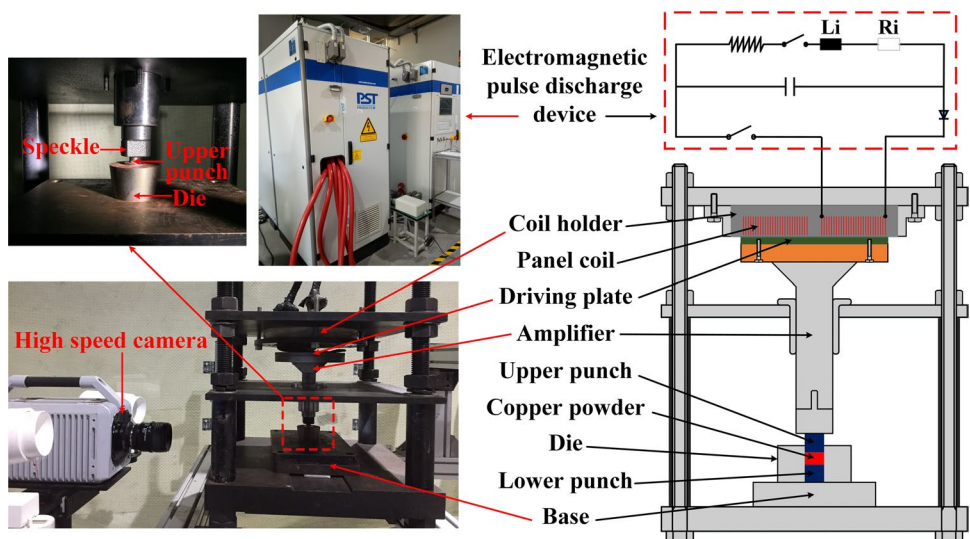


Fig. 1 SEM micrograph of copper powder

**Fig. 2** Principle and experiment device of magnetic pulse compaction



which had the maximum discharge energy of 48 kJ. The discharge energy in this work was set to 4 kJ, 5 kJ, 6 kJ, 7 kJ, 8 kJ, and 9 kJ. The upper punch pressed the powder particles under the action of electromagnetic force. The displacement of upper punch during MPC process was obtained by VIC-2D (No contact full field two-dimensional shape variable measuring system) of DIC (digital image correlation), as shown in Fig. 2. The frame rate of high speed camera was 100 k. First, the speckle on the upper punch was taken by high speed camera. Then, the pixels change of speckle was analyzed by VIC-2D software and the displacement–time curve of upper punch was obtained. After the experiments were completed, the copper compacts were removed from the die by the upper movement of the lower punch. The relative density of the copper compacts was obtained by the Archimedes drainage method (precision: 0.02 ml) and electronic balance (precision: 0.1 mg). Hardness testing was performed on the polished surfaces using a Wilson Tukon Series 1102 Vickers Hardness tester, which the load was 500 g. Three points at the upper surface, central position and lower surface of the compacts were sequentially selected for hardness testing. Microstructures at the upper surface of the copper compacts at various discharge energies were obtained by environmental scanning electron microscope (model: FEI QuANTA 200). The aqueous solution of ferric chloride hydrochloric acid with the mass ratio  $\text{FeCl}_3$ :  $\text{HCl}$ :  $\text{H}_2\text{O}$  = 5 g: 40 ml: 100 ml was selected as the etching solution. The corrosion time was about 10 s. Axial microstructures of copper compacts were obtained by metallurgical microscope (model: caikon DMM-400C) and upright digital microscope (model: OLYMPUS DSX510). The microstructures obtained by upright digital microscope were used to validate the results of finite element simulation.

### 3 Finite Element Simulation Modeling

Finite element simulation was an effective method to study the powder compaction process [22, 23]. An et al. [15] used the continuum models to simulate the powder compaction process, so the similar modeling method was used for simulation in this study. In order to observe the variation tendency of the relative density, strain and stress of powder body and the spring back behavior of copper compacts, a finite element model was established by the finite element software MSC Marc, as shown in Fig. 3.

In finite element simulation, the mesh division of the powder body could affect the simulation accuracy and the computation time. The effect of different mesh divisions on the equivalent stress of the powder body is shown in Fig. 4. The finite element model at various discharge energies was the same. Therefore, the finite element model at discharge energy 4 kJ was selected to study the mesh convergence. In addition, the equivalent stress in Fig. 4 referred to the stress

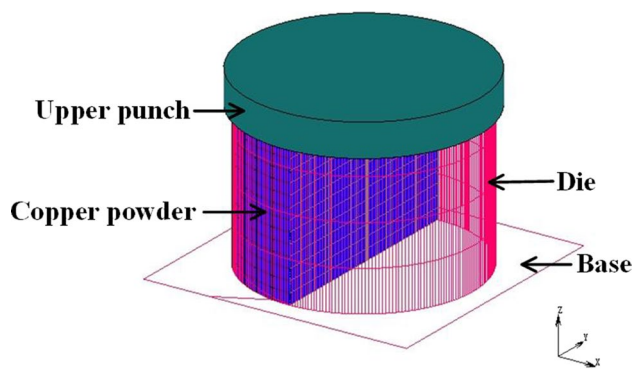


**Fig. 3** Finite element model of MPC process

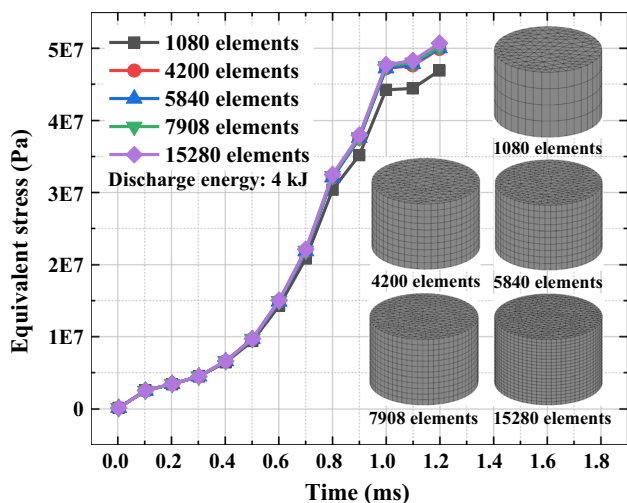


**Fig. 4** Variation of the equivalent stress of the powder body at various mesh divisions

value at the upper edge of the powder body. As can be seen from Fig. 4, the change of the equivalent stress-time curve was slight when the element number was greater than 4200. Therefore, the mesh division of the powder body which contained 7908 elements could satisfy the simulation accuracy. It should be noted that the further refinement of the element had little effect on the simulation results and was time consuming [24].

The copper powder was set to a deformable body, and the upper punch, die, base were set to rigid bodies. The powder body was divided into 7908 elements and 4706 nodes. The Delaunay method was used to generate a two-dimensional triangular element with the side length of 0.5 mm. The relax method was used to reduce the distortion of the elements and improve the quality of the elements. Then, the two-dimensional triangular element was expanded to a three-dimensional element with the height of 0.5 mm. The element type was defined as a fully integrated pentahedral element type 136. The relationship between Young’s modulus, Poisson’s ratio and relative density were defined by the table option and then applied to the material. In addition, the value of thermal conductivity, thermal expansion coefficient and specific heat of copper at different temperatures were determined,

as shown in Table 1. These data were entered as material parameters in the finite element model.

The contact between the deformed body and the rigid body was defined by the contact table. The friction model used in the simulation was the modified coulomb friction model [15]. The friction coefficient of copper powder and carbon steel was set to 0.35. The initial relative density and temperature were defined by the initial condition option. The motion of the upper punch was controlled by applying the displacement–time curves, as shown in Fig. 5. Demolding process was achieved by applying a displacement–time curve to the lower punch and the demolding speed was 1 mm/s. Two analysis conditions were defined to simulate the compaction and demolding processes of the powder body. The Newton–Raphson method with strain correction was selected as the iterative method. The convergence tolerance of the relative residual stress and the relative displacement were set to 0.1, and automatic conversion was allowed. Large strain and updated Lagrange method options were selected to analysis the job. The analysis step for compaction was set to 0.01 ms, and the analysis step for demolding was set to 0.03 s.

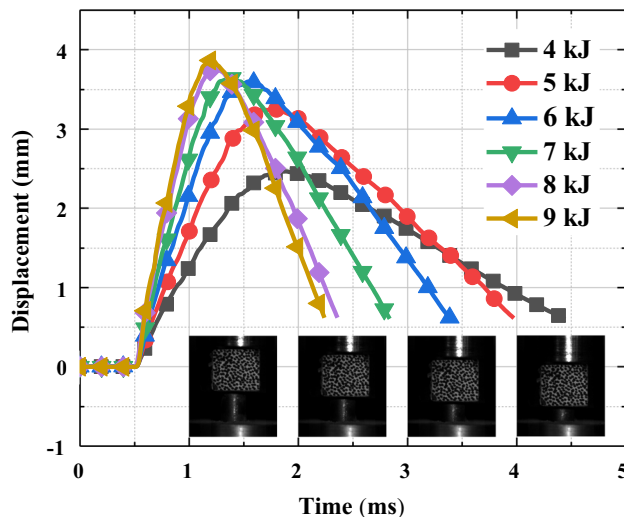


**Fig. 5** Displacement-time curves of upper punch at various discharge energies

**Table 1** Copper material parameters [25]

Temperature (K)	293	373	473	573	673	773	873	973
Thermal conductivity (w/m K)	392	376	360	341	324	305	286	280
Specific heat (J/kg K)	385	393	414	422	431	443	456	468
Thermal expansion coefficient ( $10^{-5}/K$ )	1.7	1.76	1.8	1.9	2	2.1	2.14	2.2

The yield criterion proposed by Shima et al. [26] was selected and applied to the material. The yield criterion of the powder material can be obtained as following:

$$f = 1/\gamma \left\{ 1/2 \times \left[ (\sigma_1 - \sigma_2)^2 + (\sigma_2 - \sigma_3)^2 + (\sigma_3 - \sigma_1)^2 \right] + (\sigma_m/\beta)^2 \right\}^{1/2} - \sigma_0 \quad (1)$$

where  $f$  is the plastic yield strength,  $\gamma$  is the function of density,  $\sigma_m$  is the hydrostatic pressure,  $\beta$  is the function of the relative density of the porous material.  $\gamma$ ,  $\beta$  were functions of relative density, the expressions were as following:

$$\gamma = (q_1 + q_2 \times \rho^{q_3})^{q_4} \quad (2)$$

$$\beta = (b_1 + b_2 \times \rho^{b_3})^{b_4} \quad (3)$$

According to the copper powder compaction experiment, Shima et al. [26] obtained the following relationship:

$$\gamma = \rho^{2.5} \quad (4)$$

$$\beta = 1/2.49 \times (1 - \rho)^{-0.514} \quad (5)$$

By comparing the four equations mentioned above, the parameters needed for simulation could be obtained. Which were  $q_1 = 0$ ,  $q_2 = 1$ ,  $q_3 = 1$ ,  $q_4 = 2.5$ ;  $b_1 = 5.946$ ,  $b_2 = -5.946$ ,  $b_3 = 1$ ,  $b_4 = -0.514$ . The McAdam's Young's modulus model [27] and the Ren's Poisson's ratio model [28] was selected for finite element simulation. The expressions were as following:

$$E = E_0(1 - p)^{3.4} \quad (6)$$

$$\nu = 0.35e^{-12.5(1-\rho)^2} \quad (7)$$

where  $E_0$  represents the Young's modulus of the dense materials,  $p$  is porosity,  $\nu$  represents the Poisson's ratio,  $\rho$  represents the relative density.

## 4 Results and Discussions

### 4.1 Microstructure Analysis

The appearance of copper compacts at various discharge energies are shown in Fig. 6. The height of the copper compacts decreased with the increase of discharge energy. The microstructures at the upper surface of the copper compacts at various discharge energies are shown in Fig. 7. It could be observed from Fig. 7a that there were large pores when the discharge energy was 4 kJ. In addition, the powder particles were not sufficiently deformed. The pores were gradually reduced when the discharge

energy increased from 5 kJ to 7 kJ. The slope of displacement–time curves in Fig. 5 increased with the increase of discharge energy, which indicated that the compaction

velocity was improved. Therefore, the impact force was increased with the increase of compaction velocity and the pores were decreased by the increased compaction force. As can be seen from Fig. 7e and f, there were almost no pores in the microstructures when the discharge energies were 8 kJ and 9 kJ. It meant that the density of copper compacts were close to the theoretical density when the discharge energy was greater than 8 kJ.

In order to further analyze the effect of discharge energy on the deformation of powder particles, axial microstructures of copper compacts were obtained, as shown in Fig. 8. It could be observed from Fig. 8d–f that there were obvious fine particle zones in the copper compacts. It was analyzed that copper powder particles were subjected to a high compaction force and high compaction velocity during a short period of time [8]. The slope of displacement–time curves in Fig. 5 indicated that the compaction velocity have reached 8 m/s. According to the relationship between momentum and impulse, the impact force was huge. In addition, MPC was a kind of dynamic compaction method with high forming rate and the stress wave could propagate in the powder particles [29]. The deformation and rearrangement of the particles cloud be improved within very short time by the high compaction pressure of MPC process [30]. Due to the high degree of deformation and huge impact force in a very short time, the powder particles were crushed and then filled into the pores between the particles. Based on the Hall–Petch formula [31], the strength of the copper compacts could be improved by the refined particles.

### 4.2 Relative Density Analysis

The microstructures in Figs. 7 and 8 indicated that the relative density increased with the increase of discharge energy. Yan et al. [32] used a new quantity, impact energy per mass,

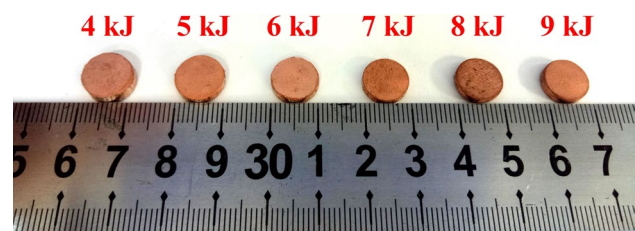
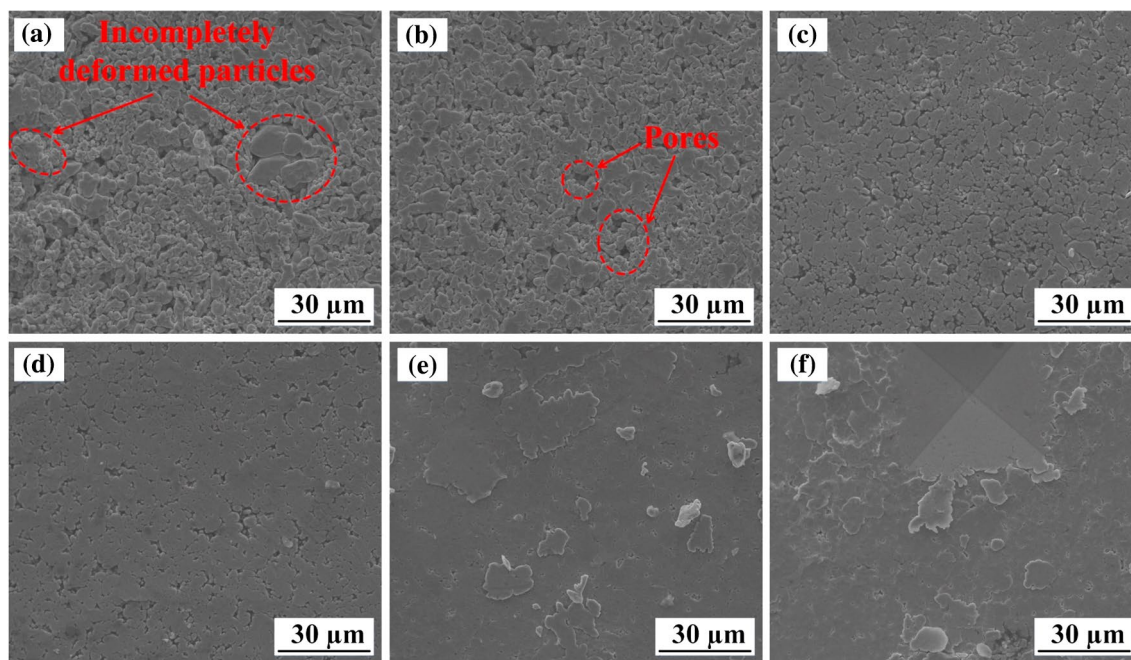


Fig. 6 Appearance of copper compacts at various discharge energies



**Fig. 7** Microstructures at the upper surface of the copper compacts at various discharge energies: **a** 4 kJ, **b** 5 kJ, **c** 6 kJ, **d** 7 kJ, **e** 8 kJ, **f** 9 kJ

to analyze the forming effects. In order to further analyze the effects of discharge energy on the relative density of copper compacts, the discharge energy per unit mass was also used for analysis. The equation for counting the discharge energy per mass was as follows [32].

$$I = E/M \quad (8)$$

where  $I$  is the discharge energy per mass,  $E$  is the discharge energy,  $M$  is the mass of the powder body. The calculation results are shown in Fig. 9. The relative density increased rapidly and then improved slowly with the increase of discharge energy per mass. Based on the raw data and the fitting curve, the relative density of copper compacts could reach to 97.8% when the discharge energy per mass was 7. In addition, the discharge energy per mass was greater than the research data of Yan et al. [32]. It meant that the powder particles subjected a huge compaction force during MPC process. Therefore, the density could be improved rapidly in a short period of time.

Relative density was an important quality parameter of copper compacts and was therefore used to validate the simulation results. Four different regions of the axial microstructures of copper compact at 7 kJ were selected to compare the simulation results at the same discharge energy. It should be noted that the finite element models used at various discharge energies were the same. Therefore, just one model needed to be selected and compared with the experiment, and the comparison results were

applicable to the other models. The software Image J was used to calculate the pore density of the microstructures. Then, the pore density was used to verify the reliability of the simulation results. The pore density of the microstructures and the simulation results are shown in Fig. 10. The relative density comparison results of the experiment and the simulation are shown in Fig. 11. From the analysis of Figs. 10 and 11, the simulation results had a same tendency with the experiment data. Therefore, the simulation results could be used to analyze the powder compaction behavior.

In order to further analyze the effects of discharge energy on the variation tendency of the relative density, the relative density cloud images at the middle stage of the compaction were selected, as shown in Fig. 12. When the discharge energies were 4 kJ, the relative density cloud images showed a clear gradient. The arrows in Fig. 12 indicated the variation tendency of the relative density of powder body during MPC process. The relative density at the upper edge of the powder body was the highest, which was consistent with the Fig. 10a. It was analyzed that the powder particles at the upper edge of the powder body were subjected to the frictional force of the inner wall of the die. Thus the powder particles were not easily to move in the axial direction. Due to the frictional force of the upper punch, it was difficult for the powder particles at the upper edge to laterally move. These two factors caused the powder particles at the upper edge of the powder body to accumulate, and the relative density value was the highest. The relative density at the

**Fig. 8** Axial microstructures of the copper compacts at various discharge energies: **a** 4 kJ, **b** 5 kJ, **c** 6 kJ, **d** 7 kJ, **e** 8 kJ, **f** 9 kJ

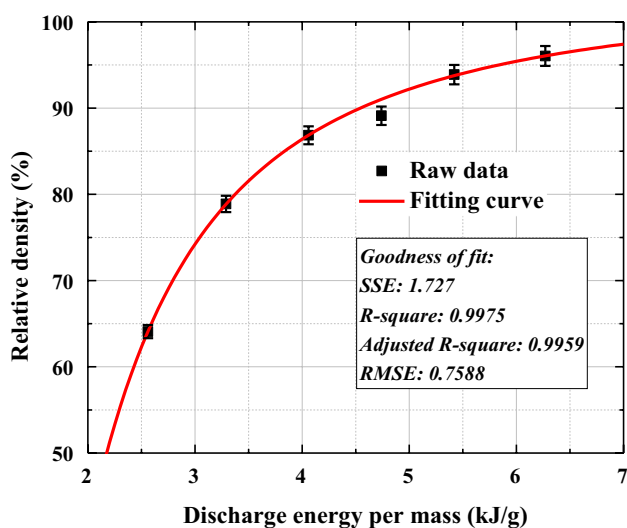
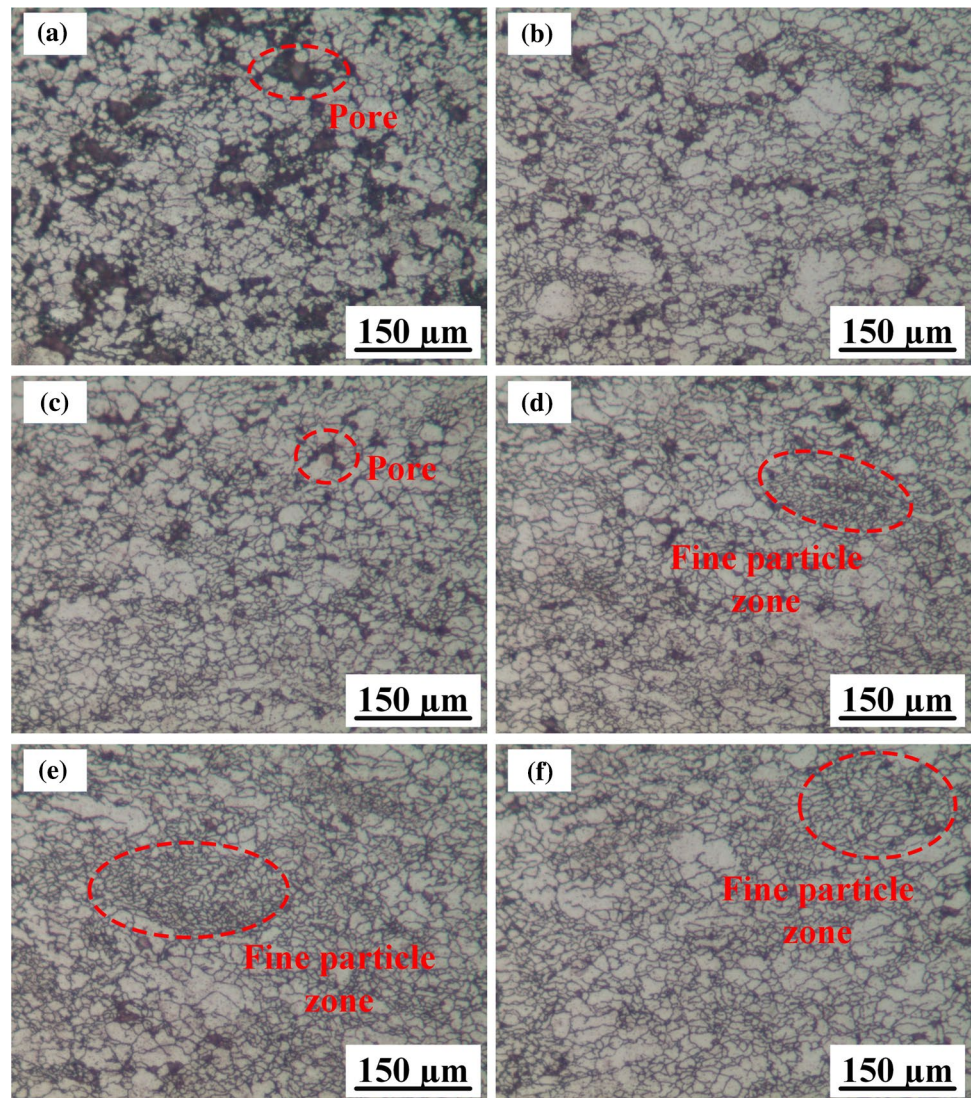


**Fig. 9** Relationship between relative density and discharge energy per mass

upper center was greater than that at the lower center. It was because the compaction force was gradually decreased along the compaction direction. However, the difference of relative density was small and further reduced as the discharge energy increased. The calculation results in Fig. 10c and d showed that the difference of relative density was just 0.4% at the discharge energy 7 kJ. The relative density at the lower edge of the powder body was the lowest. It was analyzed that the powder particles at the lower edge were subjected to the minimum compaction force. At the same time, the presence of friction force caused less powder particles to flow to this zone. Therefore, the pore density in this area was higher and the relative density in Fig. 10b was the lowest. When the discharge energy was greater than 7 kJ, the gradient of relative density was basically disappeared and the relative density showed a more uniform distribution. It meant that the powder bodies could have a uniform density distribution within 0.6 ms when the discharge energy of MPC technique

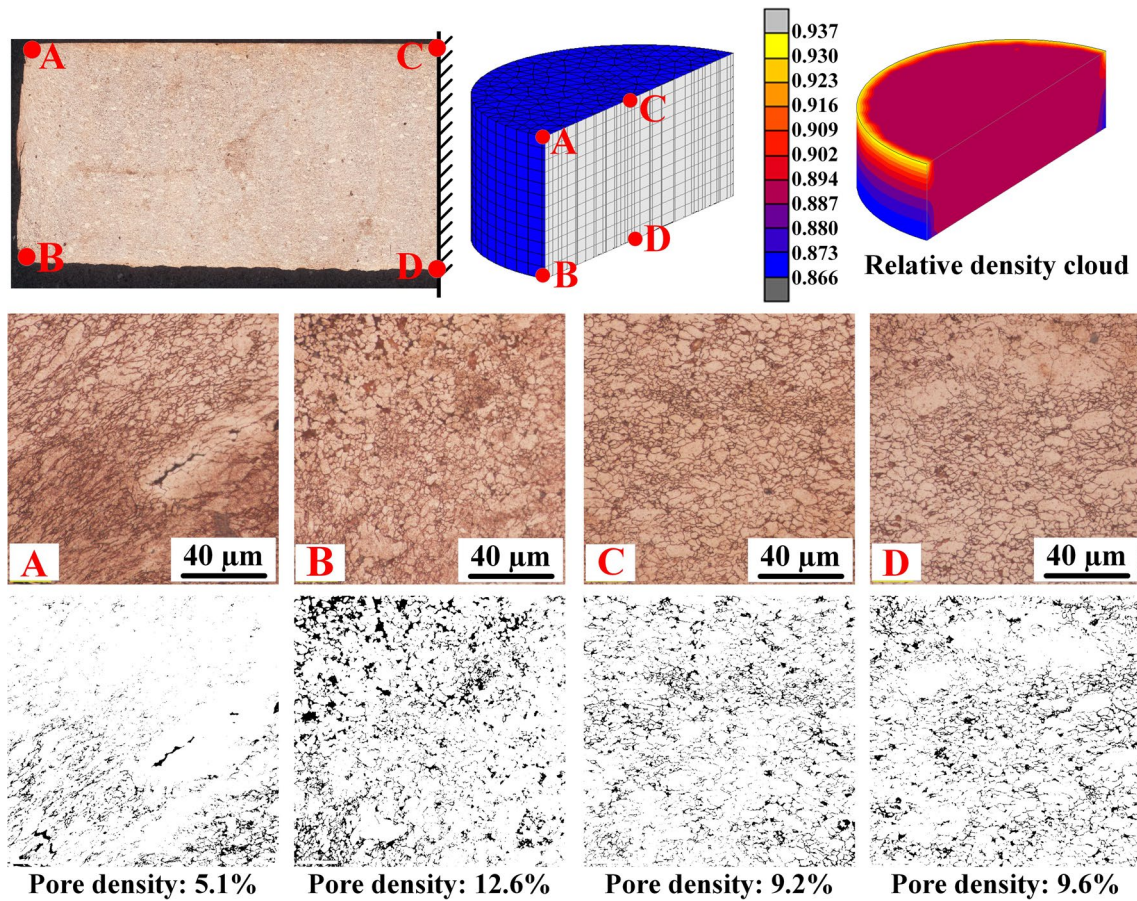


Fig. 10 Pore density of microstructures and relative density cloud of copper compact at discharge energy 7 kJ

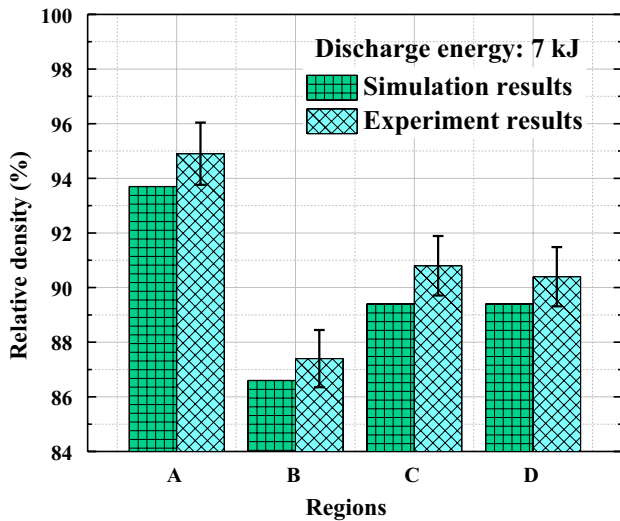


Fig. 11 Relative density comparison results of the experiment and the simulation at discharge energy 7 kJ

was greater than 7 kJ. The effect of frictional force on the powder particles would be weakened.

### 4.3 Stress and Strain Analysis

The equivalent stress cloud images of powder bodies at the same compaction moment at various discharge energies are shown in Fig. 13. The arrows in Fig. 13 indicated the variation tendency of the equivalent stress of powder body during MPC process. Specifically, stress concentration was occurred at the upper edge of the powder body, and propagated to the upper center, lower edge and middle position of the powder body. It was analyzed that the decrease of stress along the compaction direction was caused by the friction force. At the same compaction moment, the peak stress rapidly increased from 14.8 MPa to 3880.8 MPa with the increase of discharge energy. When the discharge energy was greater than 7 kJ, the equivalent stress was significantly greater than the yield stress of copper. It meant that the pores were drastically reduced and particles were mainly undergoing deformation, which was corresponding to the analysis of Figs. 7 and 8. The gradient of stress was reduced and the



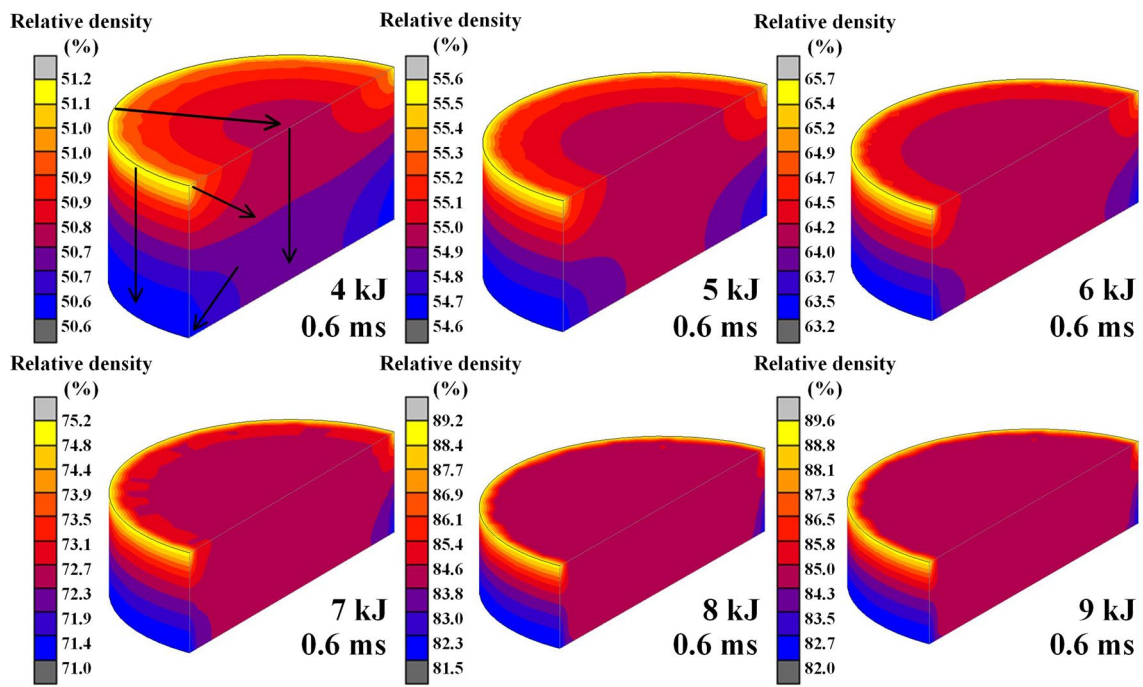


Fig. 12 Relative density cloud images of powder bodies at the same compaction moment at various discharge energies

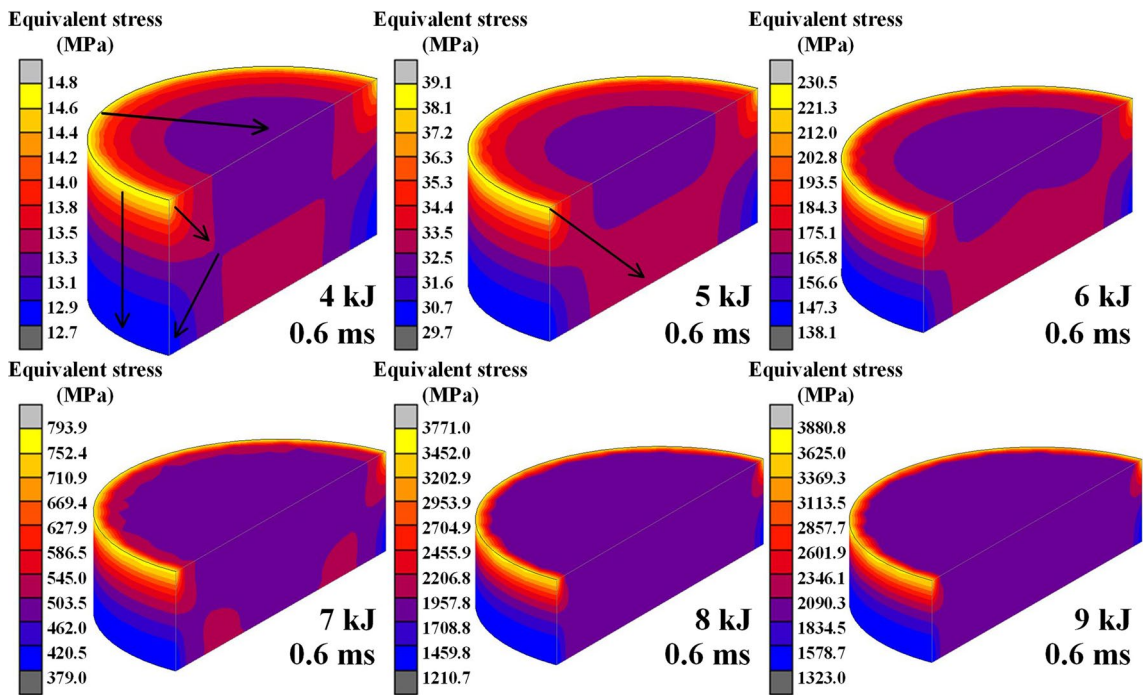


Fig. 13 Equivalent stress cloud images of powder bodies at the same compaction moment at various discharge energies

distribution of stress was relatively uniform. It indicated that the powder body could have a uniform stress distribution in a short period of time when the discharge energy was greater than 7 kJ.

Powder body was considered to be a compressible continuum, the volume strain of powder body at various discharge energies could be used to analyze the compaction characteristics. Based on Huang Pei-yun equation, the volume strain of powder body could be calculated by the following equation [33].

$$\varepsilon = \ln \left[ \frac{(\vartheta_0 - \vartheta_m)}{(\vartheta - \vartheta_m)} \right] \tag{9}$$

where  $\vartheta_0$  is the initial volume of the powder body,  $\vartheta_m$  is the volume of copper compacts when the relative density was theoretical density,  $\vartheta$  is the volume of the copper compacts at the end of compaction. The calculation results are shown in Fig. 14. The volume strain at various discharge energies could be divided into three stages: I, II, III. It was analyzed that the rapidly increase of volume strain in stage I was related to the pores in the compacts. It could be observed from Figs. 7 and 8 that there were many pores in microstructures when the discharge energy was 4 and 5 kJ. In addition, the relative density of compacts in stage I was lower than 80%, as shown in Fig. 9. Therefore, the deformation resistance of powder body was relatively small. During stage II, the deformation resistance of powder body was increased. The particles were mainly undergoing deformation after the pores were greatly reduced. Thus, the increase of volume strain was slight. When the discharge energies were greater than 7 kJ, the compaction velocity was fast and the compaction force was increased. The equivalent stress in Fig. 13 indicated that the stress was greater than yield stress. The particles were fully deformed and the fine particles were filled in the pores, as shown in Fig. 8. Therefore, the volume strain was increased.

In order to further analyze the effects of discharge energy on the variation tendency of strain during MPC process, the equivalent strain cloud images at the same compaction moment were selected, as shown in Fig. 15. The arrows in

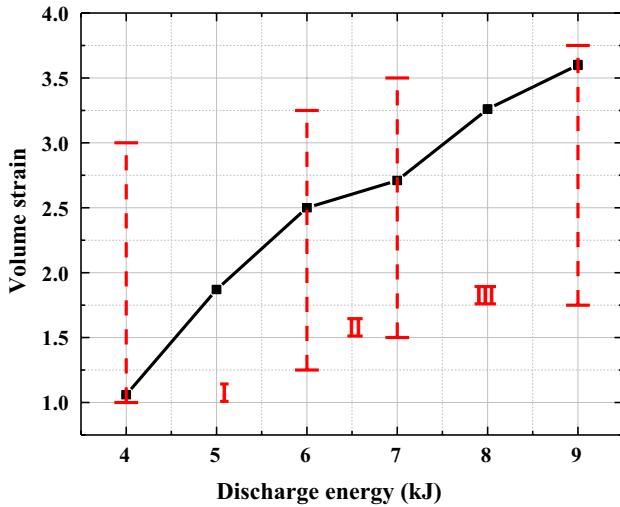


Fig. 14 Volume strain of powder bodies at various discharge energies

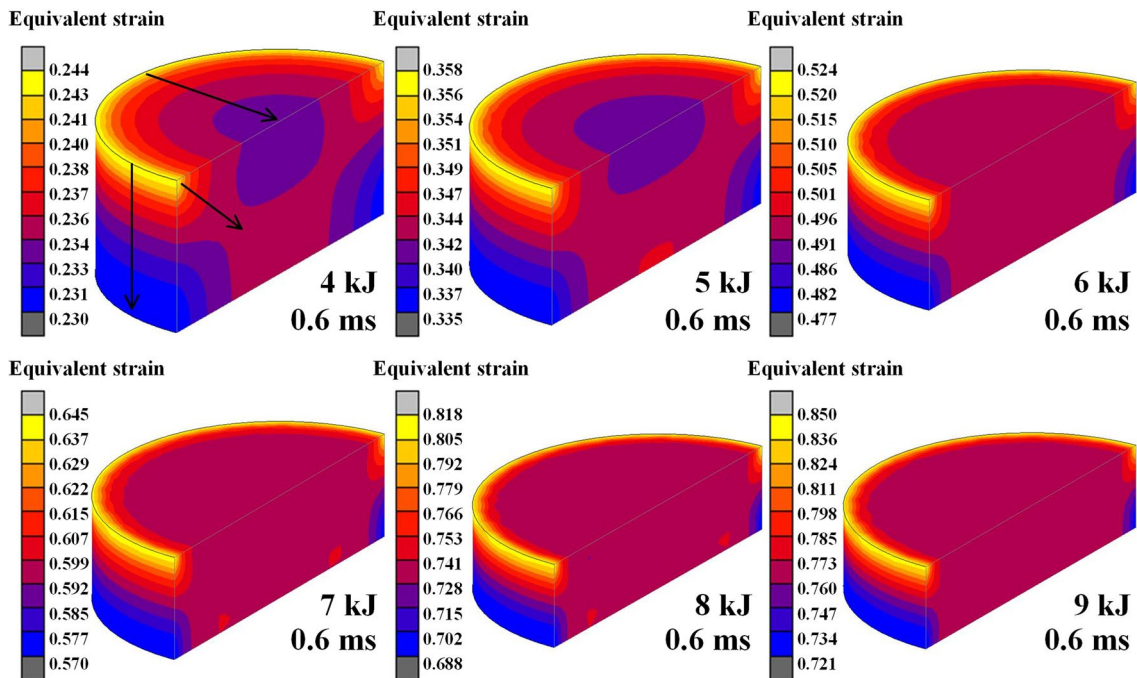
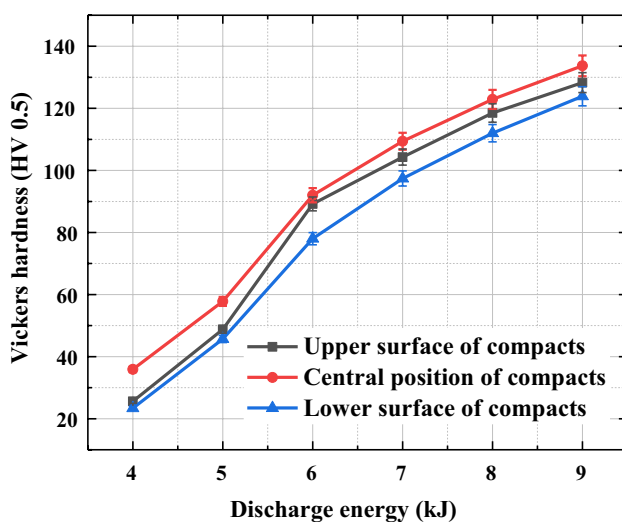


Fig. 15 Equivalent strain cloud images of powder bodies at the same compaction moment at various discharge energies

Fig. 15 indicated the variation tendency of the equivalent strain of powder body during MPC process, which was similar with that in Fig. 13. The equivalent strain at the upper edge of the powder body was the highest. It meant that the particles at this position were subjected to a high pressure and had a high degree of deformation. The equivalent strain at the lower edge of the powder body was the lowest. It was analyzed that the particles at this position were subjected to the lowest force and particles were not easily to flow to this position. The calculation of pore density in Fig. 10 showed the analysis was correct. When the discharge energy was greater than 7 kJ, the gradient of equivalent strain was basically disappeared. It was analyzed that the equivalent stress was rapidly increased. In addition, the compaction force during MPC process transmitted down to the bottom of powder body through stress wave before the upper powders were pressed completely [29]. Therefore, the strain distribution of powder body could be more uniform in a short period of time as the discharge energy increased.

#### 4.4 Micro Hardness Analysis

Micro hardness of copper compacts was measured to analyze the effect of discharge energy on the mechanical strength of copper compacts. The micro hardness of copper compacts at various discharge energies are shown in Fig. 16. It was observed that the micro hardness of copper compacts increased from 30 HV0.5 to 130 HV0.5 with the increase of discharge energy. There were large pores in the compacts when the discharge energy was 4 and 5 kJ, as shown in Fig. 8. It was analyzed that the pores would impair the strength of compacts. Therefore, the micro hardness was low when the discharge energy was 4 and 5 kJ. The pores



**Fig. 16** Micro hardness of copper compacts at various discharge energies

were reduced and the bonding strength between particles was improved with the increase of discharge energy. In addition, from the analysis of Fig. 9, the fine particle zones were formed inside the compacts and the mechanical strength could be improved by the fine particles [34]. It was observed that the micro hardness at the central position of the copper compacts was highest at various discharge energies. It was analyzed that the powder particles in the central position of compacts had a higher degree of rearrangement and deformation compared with the particles at the upper and lower surface. Specifically, the particle at the lower surface had the smallest displacement and was only squeezed by the particles above it. Although the particle at the upper surface had ample displacement, it was only affect by the particles below it. However, the particle in the central position was squeezed by the particles in all directions around it. Therefore, the particles in the central position had a higher degree of deformation and the bonding force between particles was higher. In addition, the fine particles zones formed in the central position had a positive effect on the strength of the compacts.

Michel et al. [35] analyzed the relationship between relative density and Vickers hardness of steel part. Results showed that there was a linear relationship between the relative density and the logarithm of Vickers hardness. The method proposed by Michel et al. [35] was used to analyze the relationship between relative density and Vickers hardness of copper compacts, as shown in Fig. 17. It was observed from Fig. 17 that there was a linear relationship between the relative density and the logarithm of Vickers hardness of copper compacts.

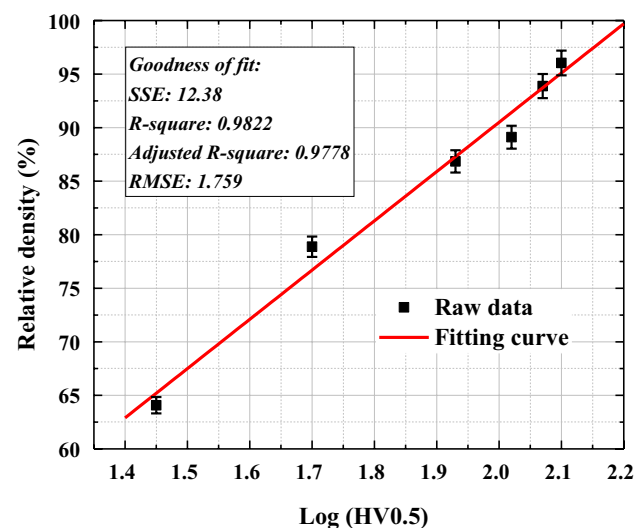


**Fig. 17** Relationship between relative density and logarithm of Vickers hardness of copper compacts

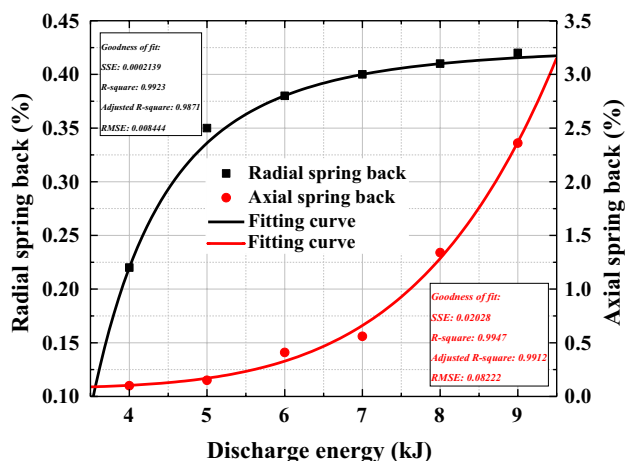


**Fig. 18** Relationship between spring back of copper compacts and discharge energy

#### 4.5 Spring Back Analysis

Spring back was caused by the release of elastic inner stress. The spring back of copper compacts ( $\zeta$  (%)) was measured according to the following equation [36, 37].

$$\zeta(\%) = 100 \times (\Phi - \Phi_0) / \Phi_0 \quad (10)$$

where  $\Phi$  is the diameter or height of the copper compacts after demolding,  $\Phi_0$  is the diameter or height of the copper compacts at the end of compaction. The radial spring back and axial spring back of copper compacts at various discharge energies were calculated by Eq. 10, as shown in Fig. 18. The radial spring back and the axial spring back of copper compacts increased from 0.1 and 0.1 to 0.42% and 2.36% with the increase of discharge energy, respectively. It was observed from Figs. 7 and 8 that there were visible pores in the compacts when the discharge energy was 4 and 5 kJ. Although the contact state of particles was changed by the release of elastic inner stress, the existence of pores could give space for the changed contact state. In addition, Figs. 13 and 15 indicated that the compacts were consolidated in a short period of time and the equivalent stress was relatively small. Therefore, the radial and axial spring back was low when the discharge energy was 4 and 5 kJ. When the discharge energy was increased, the pores were significantly reduced and the equivalent stress was drastically increased, as shown in Figs. 8 and 13. Therefore, the change of contact state caused a higher volume expansion. Besides, the volume expansion was mainly occurred before the compacts were demolded. Thus, the axial spring back value was greater than the radial spring back and the growth rate of axial spring back was also higher. The increase of

micro hardness in Fig. 16 indicated that the bonding strength between particles was improved. The high bonding strength between particles had a positive effect on the reduction of spring back. The radial spring back value tended to be a stable value with the increase of discharge energy. Although the growth rate of axial spring back was high, it should be no more than 3.5%. It was because when the discharge energy was 9 kJ, the relative density of copper compact was very close to the dense body.

## 5 Conclusions

The powder compaction characteristics and spring back behavior of copper compacts were investigated. The microstructure, relative density, micro hardness, strain and stress of copper compacts were analyzed by experiments and FEM simulation. The relationship between discharge energy and spring back was researched by numerical calculation. Some results were in the following conclusions.

1. The MPC method had the advantages to refine powder particles. Discharge energy per mass indicated that the powder particles subjected a huge compaction force during MPC process. The copper compacts with a uniform density distribution could be obtained by MPC process.
2. The volume strain at various discharge energies could be divided into three stages: I, II, III. Stress concentration was occurred at the upper edge of the powder body, and propagated to the upper center, lower edge and middle position of the powder body. The powder body could have a uniform strain distribution in a short period of time when the discharge energy was greater than 7 kJ.
3. There was a linear relationship between the relative density and the logarithm of Vickers hardness. The axial and radial spring back both increased with the increase of discharge energy. When the discharge energy was 9 kJ, the axial and radial spring back was 2.36% and 0.42%.

**Acknowledgements** This project is supported by National Natural Science Foundation of China (No. 51975202) and the Natural Science Foundation of Hunan Province (2019JJ30005).

**Data Availability** The raw/processed data required to reproduce these findings cannot be shared at this time due to technical or time limitations.

#### Compliance with Ethical Standards

**Conflict of interest** The authors declare that they have no conflict of interest.

## References

1. L. Bolzoni, F. Yang, *J. Mech. Behav. Biomed.* **97**, 41–48 (2019)
2. H. Kulkarni, V.V. Dabhade, *J. Manuf. Process.* **44**, 1–18 (2019)
3. Z. Meng, S. Huang, W. Sun, *J. Wuhan Univ. Technol.* **22**, 714–717 (2007)
4. Z. Tang, D. Hao, K. Tao, J. Chen, J. Zhang, *J. Mater. Process. Technol.* **263**, 343–355 (2019)
5. Z. Tang, S.F. Golovashchenko, J.F. Bonnen, A.V. Mamutov, A.J. Gillard, D. Bonnen, *J. Mater. Process. Technol.* **214**(12), 2843–2857 (2014)
6. M.A. Eryomina, S.F. Lomayeva, V.V. Tarasov et al., *Met. Mater. Int.* (2019). <https://doi.org/10.1007/s12540-019-00531-9>
7. A.-G. Mamalis, A. Szalay, N. Göbl, I. Vajda, B. Raveau, *Mater. Sci. Eng. B-Adv.* **53**, 119–124 (1998)
8. H.-Y. Park, M.F. Kilicaslan, S.-J. Hong, *Powder Technol.* **224**, 360–364 (2012)
9. S. Yan, S. Huang, W. Liu, J. Hu, Yu. Lei, M. Zhou, *Powder Technol.* **306**, 1–9 (2017)
10. G.H. Lee, C.K. Rhee, M.K. Lee, W.W. Kim, V.V. Ivanov, *Mater. Sci. Eng. A-Struct.* **375**, 604–608 (2004)
11. R.C. Kyu, L. Geunhee, K. Wheung, I. Victor, A. Medvedev, A. Shtolz, S. Zayats, *J. Metastab. Nanocrystal. Mater.* **15**, 757–762 (2003)
12. X.J. Yuan, Y.X. Zhuo, H. Yin, J. Guan, D. Khan, X. Qu, *Rare Metal Mater. Eng.* **40**, 86–89 (2011). **(In Chinese)**
13. D.F. Khan, H. Yin, H. Li, Z. Abideen, Asadullah, X. Qu, M. Ellahi, *Mater. Des.* (1980-2015). **54**, 149–153 (2014)
14. V. Fartashvand, A. Abdullah, S.A.S. Vanini, *Ultrason. Sonochem.* **36**, 155–161 (2017)
15. X. An, Y. Zhang, Y. Zhang, S. Ynag, *Metall. Mater. Trans. A* **46**, 3744–3752 (2015)
16. R.S. Ransing, D.T. Gethin, A.R. Khoei, P. Mosbah, R.W. Lewis, *Mater. Design.* **21**, 263–269 (2000)
17. A. Krok, P. García-Triñanes, M. Peciar, C.Y. Wu, *Chem. Eng. Res. Des.* **110**, 141–151 (2016)
18. A.R. Khoei, *Mater. Des.* **23**, 523–529 (2002)
19. C. Deng, M. Liu, P. Molian, *Powder Technol.* **239**, 36–46 (2013)
20. J. Cui, D. Dong, X. Zhang, X. Huang, G. Lu, H. Jiang, G. Li, *Int. J. Impact Eng.* **115**, 1–9 (2018)
21. H. Jiang, T. Luo, G. Li, X. Zhang, J. Cui, *Int. J. Fatigue* **105**, 180–189 (2017)
22. L.-H. Han, P.-R. Laity, R.-E. Cameron et al., *J. Mater. Sci.* **46**, 5977–5990 (2011)
23. H. Diarra, V. Mazel, A. Boillon, L. Rehault, V. Busignies, S. Bureau, P. Tchoreloff, *Powder Technol.* **224**, 233–240 (2012)
24. M. Zhou, S. Huang, H. Jianhua, Yu. Lei, F. Zou, S. Yan, M. Yang, *Powder Technol.* **313**, 68–81 (2017)
25. J.-S. Liu, *Application of MSC. MARC in Material Processing Engineering* (China Water & Power Press, Haidian, 2010)
26. S. Shima, M. Oyane, *Int. J. Mech. Sci.* **6**, 285–291 (1976)
27. G.D. McAdam, *Tetsu to Hagane* **168**, 346–358 (1951)
28. X.P. Ren, E. Wang, W.C. Huo, *Powder Metall. Technol.* **1**, 8–12 (1992). **(In Chinese)**
29. Z.H. Meng, S.Y. Huang, M. Yang, *J. Mater. Process. Technol.* **209**(2), 672–678 (2009)
30. H.-Y. Park, M.F. Kilicaslan, S.-J. Hong, *Mater. Chem. Phys.* **141**(1), 208–215 (2013)
31. C.L. Li, Q.S. Mei, J.Y. Li, F. Chen, Y. Ma, X.M. Mei, *Scripta Mater.* **153**, 27–30 (2018)
32. Z. Yan, F. Chen, Y. Cai, *Powder Technol.* **208**(3), 596–599 (2011)
33. P.Y. Huang, *Theory of powder metallurgy*, 2nd edn. (Metallurgical industry press, Beijing, 1982), pp. 184–185
34. M.A.J. Taleghani, E.M.R. Navas, J.M. Torralba, *Mater. Design.* **55**, 674–682 (2014)
35. H. Chtourou, M. Guillot, in *Proceeding of the PM2TEC'95 Conference*
36. S. Garner, J. Strong, A. Zavaliangos, *Powder Technol.* **330**, 357–370 (2018)
37. D.F. Khan, H. Yin, H. Li, X. Qu, M. Khan, S. Ali, M.Z. Iqbal, *Mater. Des.* **50**, 479–483 (2013)

**Publisher's Note** Springer Nature remains neutral with regard to jurisdictional claims in published maps and institutional affiliations.